Nonlinear optical properties of Rb_2ZnCl_4 in the incommensurate and ferroelectric phases

R. Sanctuary, D. Jundt, J.-C. Baumert, and P. Günter
Laboratory of Solid State Physics, Swiss Federal Institute of Technology, Eidgenössische Technische Hochschule—Hönggerberg, 8093-Zürich, Zürich, Switzerland
(Received 27 December 1984)

Nonlinear optical properties of Rb_2ZnCl_4 are measured for the incommensurate and ferroelectric phases by means of second-harmonic generation experiments. In the temperature range of the ferroelectric lock-in phase, the nonlinear optical coefficients d_{33}, d_{32}, and d_{24} and the Miller δ coefficients are determined using the wedge technique and are shown to be proportional to the spontaneous polarization. In the incommensurate phase of Rb_2ZnCl_4, the order of magnitude of the second-harmonic intensity corresponding to nonlinear optical coefficients allowed by the local point-group symmetry is estimated to be at least 10^7 times smaller than the second-harmonic intensity generated in quartz and thus difficult to detect. Furthermore, it is shown that quasi-phase-matching of the fundamental and second-harmonic waves in the incommensurate phase is limited to a very small temperature range of $T_C < T < T_C + 0.01$ mK. (T_C is the incommensurate-ferroelectric phase-transition temperature.) The temperature dependence of the second-harmonic intensity in the range $T_C < T < 198$ K is explained by the occurrence of a defect-induced unipolar domain structure.

I. INTRODUCTION

Rb_2ZnCl_4 belongs to the family of tetrahedrally coordinated A_2BX_4 crystals with β-K_2SO_4 structure. It shows a succession of four phases with decreasing temperature: the paraelectric phase *Pnam*, the incommensurate phase in which the wave vector of the condensed-out soft mode $\mathbf{q}_I = [1-\delta(T)](\mathbf{a}^*/3)$ ($\delta \ll 1$, $\mathbf{a}^*$ is a reciprocal-lattice vector of the paraelectric phase) deviates slightly from the lock-in wave vector $\mathbf{q}_C = \mathbf{a}^*/3$, the commensurate improper ferroelectric, ferroelastic lock-in phase $Pna2_1$ with spontaneous polarization along the crystallographic c axis, and finally the ferroelectric low-temperature phase with monoclinic space group $A1a1$ and spontaneous polarization within the a-c plane. At normal atmospheric pressure and no applied electric field, the phase-transition temperatures are $T_I = 303$ K, $T_C = 192$ K, and $T_L = 75$ K upon cooling. The small deviation of the incommensurate soft-mode wave vector $\mathbf{q}_I$ from $\mathbf{q}_C$ results in a superlattice, the periodicity of which is an irrational fraction of the periodicity of the underlying lattice. As a consequence the translational symmetry in the direction of the incommensurate modulation is lost. The incommensurate and ferroelectric phases of Rb_2ZnCl_4 have by now been investigated using various experimental techniques such as x-ray and Raman scattering[1,2] or nuclear magnetic resonance.[3] Spontaneous polarization data and dielectric measurements are reported in Refs. 4–8. We finally carried out birefringent and electro-optic measurements in the incommensurate and ferroelectric lock-in phases of Rb_2ZnCl_4.[9–11] Optical second-harmonic–generation experiments turned out to be an efficient tool for investigating local-symmetry changes within the incommensurate phase of Rb_2ZnCl_4 as well as for studying the phase transition from the incommensurate to the commensurate ferroelectric phase. Preliminary experiments of this type have already been reported for K_2SeO_4 and $(NH_4)_2BeF_4$ crystals.[12,13] These materials belong to the same crystal family and show the same phase sequence as Rb_2ZnCl_4. Both materials, however, exhibit in the incommensurate phase a quite different nonlinear optical behavior. In this paper we report nonlinear optical experiments in the incommensurate and ferroelectric phases of Rb_2ZnCl_4. The experimental results in the incommensurate phase will be compared with various theoretical models for the nonlinear optical susceptibility. The possibility of quasi-phase-matching near T_C for light-propagation direction along the spatial modulation axis will be discussed. In the ferroelectric lock-in phase the temperature dependence of the nonlinear optical coefficients d_{33}, d_{32}, and d_{24} will be reported and compared with the temperature dependence of the spontaneous polarization. Furthermore, the contribution of field-induced electronic excitations to the low-frequency electro-optic effect will be discussed.

II. THEORETICAL

A. The nonlinear optical effect

1. Nonlinear optical coefficients

In a nonmagnetic, lossless crystal the induced electric polarization per unit volume $\mathbf{P}$ can be expanded as a power series in the electric field components E_m of the light waves propagating in the medium. A Fourier transformation of this power series in time yields

$$P_i^{(\omega_n)} = \epsilon_0(\chi_{ij}^{(\omega_n)} E_j^{(\omega_n)} + d_{ijk}^{(-\omega_n;\omega_o,\omega_p)} E_j^{(\omega_o)} E_k^{(\omega_p)} + d_{ijkl}^{(-\omega_n;\omega_q,\omega_r,\omega_s)} E_j^{(\omega_q)} E_k^{(\omega_r)} E_l^{(\omega_s)} + \cdots), \quad (1)$$

where we sum over repeated indices and where we have assumed

$$\omega_n=\omega_o+\omega_p$$

and (2)

$$\omega_n=\omega_q+\omega_r+\omega_s \ .$$

$\epsilon_0=8.854\times10^{-12}$ A s/V m is the free-space permittivity. At low light intensities, i.e., weak electric fields E_m, the polarization is linear in the field

$$P_i^{(\omega_n)}=\epsilon_0\chi_{ij}^{(\omega_n)}E_j^{(\omega_n)} \ , \tag{3}$$

where χ_{ij} is the linear susceptibility of the medium related to the principal indices of refraction by

$$\chi_{ii}=n_i^2-1 \tag{4}$$

in the principal-axis system.

The nonlinear optical polarization for third-order processes (e.g., third-harmonic generation, four-wave mixing, ...) can be written in terms of the nonlinear optical coefficients d_{ijkl} or the Miller δ coefficients,[14]

$$(P_{\rm NL})_i^{(\omega_n)}=\epsilon_0 d_{ijkl}^{(-\omega_n;\omega_q,\omega_r,\omega_s)}E_j^{(\omega_q)}E_k^{(\omega_r)}E_l^{(\omega_s)} \tag{5}$$

or

$$E_i^{(\omega_n)}=\frac{1}{\epsilon_0}\delta_{ijkl}^{(-\omega_n;\omega_q,\omega_r,\omega_s)}P_j^{(\omega_q)}P_k^{(\omega_r)}P_l^{(\omega_s)} \tag{6}$$

with

$$\delta_{ijkl}^{(-\omega_n;\omega_q,\omega_r,\omega_s)}=\frac{d_{ijkl}^{(-\omega_n;\omega_q,\omega_r,\omega_s)}}{\epsilon_0^2\chi_{ii}^{(\omega_n)}\chi_{jj}^{(\omega_q)}\chi_{kk}^{(\omega_r)}\chi_{ll}^{(\omega_s)}} \ . \tag{7}$$

Analogously, second-order processes (e.g., second-harmonic generation, optical rectification, sum-frequency generation, ...) are described by

$$(P_{\rm NL})_i^{(\omega_n)}=\epsilon_0 d_{ijk}^{(-\omega_n;\omega_o,\omega_p)}E_j^{(\omega_o)}E_k^{(\omega_p)} \tag{8}$$

or

$$E_i^{(\omega_n)}=\frac{1}{\epsilon_0}\delta_{ijk}^{(-\omega_n;\omega_o,\omega_p)}P_j^{(\omega_o)}P_k^{(\omega_p)} \ , \tag{9}$$

where

$$\delta_{ijk}^{(-\omega_n;\omega_o,\omega_p)}=\frac{d_{ijk}^{(-\omega_n;\omega_0,\omega_p)}}{\epsilon_0\chi_{jj}^{(\omega_0)}\chi_{kk}^{(\omega_p)}\chi_{ii}^{(\omega_n)}} \ . \tag{10}$$

The δ coefficients have the advantage of being nearly frequency independent, whereas the d coefficients show considerable dispersions. It has been shown[15] that the values of δ are comparable in different materials specifically in oxygen-octahedra ferroelectrics.

2. *Second-harmonic generation (SHG)*

Solving Maxwell's equations with

$$(P_{\rm NL})_i^{(2\omega)}=\epsilon_0 d_{ijk}^{(-2\omega;\omega,\omega)}E_j^{(\omega)}E_k^{(\omega)} \tag{11}$$

as a source term, we get for the second-harmonic intensity $I_{2\omega}$ in the nondepleted input approximation

$$I_{2\omega}=2\left[\frac{\mu_0}{\epsilon_0}\right]^{1/2}I_\omega^2\frac{d_{\rm eff}^2 l^2}{n_{2\omega}n_\omega^2}\omega^2 j_0^2\left[\frac{\Delta k l}{2}\right] , \tag{12}$$

where μ_0 is the permeability of free space and $j_0(x)$ is the zeroth spherical Bessel function of the first kind, or $\sin x/x$. I_ω is the intensity of the fundamental wave, l the length of the crystal in the light propagation direction, $d_{\rm eff}$ the effective nonlinear coefficient, and

$$\Delta k=k_{2\omega}-2k_\omega \ , \tag{13}$$

the phase mismatch between the fundamental and second-harmonic waves. Finally, n_ω and $n_{2\omega}$ are the refractive indices of the crystal at fundamental and second-harmonic frequency, respectively.

Introducing the coherence length

$$l_c=\frac{\pi}{|\Delta k|}=\frac{\pi c}{2|n_{2\omega}-n_\omega|\omega} \ , \tag{14}$$

where c is the free-space velocity of light, it follows from (12) that l_c is a measure of the maximum interaction length that constructively contributes to the second-harmonic intensity. It should be noted that relation (12) was calculated under the plane-wave approximation for the fundamental and second-harmonic waves propagating in the same direction.

The nonlinear optical properties of Rb_2ZnCl_4 were measured using the wedge technique described by Boyd *et al.*[16] Translation of a crystal wedge perpendicular to the fundamental laser beam yields the following dependence of the second-harmonic light power on the position y:

$$P_{2\omega}(y)=Kd_{\rm eff}^2 l_c^2 P_\omega^2\frac{1}{(n_\omega+1)^4(n_{2\omega}+1)^2}\times\{1-[\cos(2\varphi)]e^{-(\pi\eta/4)^2}\} \ , \tag{15}$$

where P_ω is the fundamental power and K a constant depending essentially on the parameters of the laser beam. The phase mismatch for the translating wedge (wedge angle θ) is

$$\varphi=\varphi_0+\frac{\pi y\tan\theta}{2l_c} \ , \tag{16}$$

where we have assumed normal incidence. We write

$$\eta=\frac{w_0\tan\theta}{l_c} \ , \tag{17}$$

the beam-width parameter with w_0 describing the beam waist inside the crystal.

B. The incommensurate phase of Rb_2ZnCl_4

In the incommensurate phase of Rb_2ZnCl_4 the soft mode belongs to a two-dimensional irreducible representation[17] and a Lifshitz invariant[17] is allowed by symmetry. Expressing the transition parameters p and q in terms of the polar coordinates $A(x)$ and $\phi(x)$,

$$p(x)=A(x)\cos\phi(x), \quad q(x)=A(x)\sin\phi(x) \ , \tag{18}$$

a Landau expansion of the free-energy density yields in the continuum limit

$$g(x)=\frac{\alpha}{2}A^2+\frac{\beta_1}{4}A^4+\frac{\beta_2}{6}A^6\cos(6\phi) -\sigma A^2\frac{d\phi}{dx}+\frac{\kappa}{2}\left[A^2\left[\frac{d\phi}{dx}\right]^2+\left[\frac{dA}{dx}\right]^2\right]+\cdots , \tag{19}$$

where $\alpha=\alpha_0(T-T_0)$ is the only temperature-dependent coefficient. The first two terms represent the standard Landau expansion in a homogeneous crystal. The β_2 term represents the anisotropy energy responsible for the lock-in transition at T_C and has six minima for $0<\phi<2\pi$. The σ term is the Lifshitz invariant inducing the transition to the incommensurate phase and the κ term represents the elastic energy stabilizing the homogeneous phase. The minimization of the free energy

$$\mathcal{G}=\frac{1}{L}\int_0^L g(x)dx \tag{20}$$

is a variational problem leading to the Euler-Lagrange equations

$$\beta_2 A^6\sin(6\phi)=\frac{d}{dx}\left[A^2\left[\sigma-\kappa\frac{d\phi}{dx}\right]\right], \tag{21}$$

$$\kappa\frac{d^2A}{dx^2}=A\left[\alpha+\beta_1A^2-2\sigma\frac{d\phi}{dx}+\kappa\left[\frac{d\phi}{dx}\right]^2+\beta_2A^4\cos(6\phi)\right]. \tag{22}$$

1. The plane-wave approximation

Close to the paraelectric-incommensurate phase transition the anisotropy term is small and can be neglected relative to the Lifshitz term. Assuming the constant-amplitude approximation $dA/dx=0$ (Ref. 18), the phase equation (21) yields

$$\phi\cong qx , \tag{23}$$

where

$$q=\sigma/\kappa \tag{24}$$

is the wave number of the incommensurate modulation wave. As a consequence, the transition parameters p and q are sinusoidally modulated and so are all the physical properties of the crystal. The temperature dependence of the amplitude A can be deduced from Eq. (22),

$$A=\left[\frac{\alpha_0}{\beta_1}(T_I-T)\right]^{1/2}, \tag{25}$$

where

$$T_I=T_0+\sigma/\alpha_0\kappa \tag{26}$$

is the paraelectric-incommensurate phase-transition temperature.

2. The multisoliton limit

It is clear from relation (25) that, with decreasing temperature, the amplitude A of the order parameter increases and the anisotropy term in the free-energy density can no longer be neglected. In the low-temperature part of the incommensurate phase the plane-wave approximation consequently breaks down and is replaced by the multisoliton limit. The phase ϕ is now a solution of the sine-Gordon equation

$$\frac{d^2\phi}{dx^2}+\frac{\beta_2}{\kappa}A^4\sin(6\phi)=0 , \tag{27}$$

which can immediately be derived from the phase equation (21) assuming the validity of the constant-amplitude approximation. The solutions of this nonlinear differential equation can be written in the form

$$x=\frac{\kappa}{2\gamma}F(k,3\phi) , \tag{28}$$

where

$$k=A^2\left[\frac{\beta_2}{3\gamma}\right]^{1/2}, \tag{29}$$

and

$$F(k,3\phi)=\int_0^{3\phi}\frac{d\phi}{[1-k^2\sin^2(3\phi)]^{1/2}} \tag{30}$$

is an incomplete elliptical integral of the first kind. The integration constant γ can be obtained from the condition

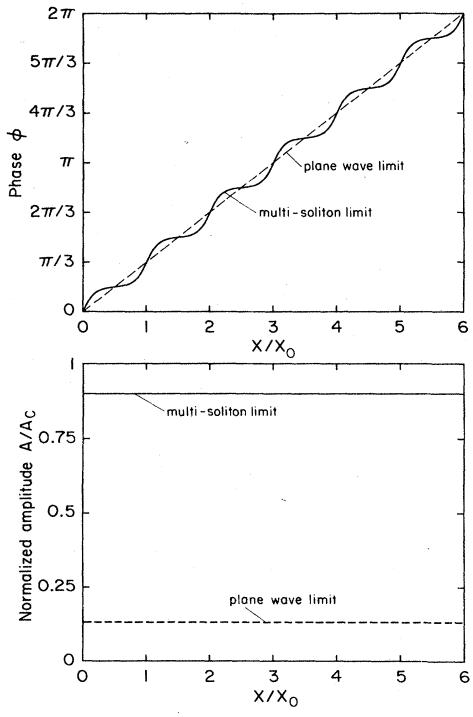

FIG. 1. Normalized amplitude A/A_c and phase ϕ of the order parameter as a function of the reduced distance x/x_0 (x_0 is the intersoliton distance, A_c the amplitude of the order parameter at the phase transition temperature T_c).

$d\mathcal{G}/d\gamma=0$.

In Fig. 1 we have plotted the spatial dependence of A and ϕ for the plane-wave approximation and the multisoliton limit, respectively. In the multisoliton limit one can see that commensurate regions—where the phase is nearly constant—are separated by a regular array of domain walls—or phase solitons—where the phase changes rapidly by an amount of $\pi/3$. As a consequence, higher harmonics must be included to describe the modulation of the physical properties of Rb_2ZnCl_4 in the low-temperature part of the incommensurate phase.

C. Spontaneous polarization of Rb_2ZnCl_4 in the incommensurate and ferroelectric lock-in phase

In the presence of an electric dc field E applied along the crystallographic c direction, the free-energy density becomes

$$g^E=g+\frac{1}{2\chi}P^2-PE+2\zeta A^3P\cos(3\phi)\ , \tag{31}$$

where g is given in (19) and P is the dielectric polarization. The ζ term resulting from the coupling of the polarization to the order parameter contributes also to the free-energy density in the absence of an electric field.

Minimizing g^E with respect to P yields

$$P=\chi E-2\zeta\chi A^3\cos(3\phi)\ . \tag{32}$$

Putting $E=0$ we get the spontaneous polarization

$$(P_S)_3=2\zeta\chi A^3\cos(3\phi)\ . \tag{33}$$

In the incommensurate phase, because of the antisymmetry of the phase ϕ relative to the soliton centers, regions with positive and negative spontaneous polarization have equal length and $(P_S)_3=0$ on a spatial average. Levstik *et al.*[6] have shown that the phase solitons can be deformed by an electric field in such a way that the antisymmetry of $\phi(x)$ around each soliton center is lost. This leads to the compression of regions with positive spontaneous polarization and to the extension of domains with opposite polarization or vice versa. Consequently, the incommensurate structure becomes polar by applying an electric field.

In the ferroelectric lock-in phase

$$\frac{d\phi}{dx}=\frac{dA}{dx}=0 \tag{34}$$

and, using Eq. (32), the free-energy density g^E can be written as

$$g^E=\frac{\alpha}{2}A^2+\frac{\beta_1}{4}A^4+2\zeta\chi EA^3\cos(3\phi)-2\hat{\gamma}A^6\cos^2(3\phi)\ , \tag{35}$$

where

$$\hat{\gamma}=\zeta\chi-\frac{\beta_2}{2}\ . \tag{36}$$

It is easy to see that g^E has minima for

$$\cos(3\phi)=\pm1\ . \tag{37}$$

The spontaneous polarization then becomes

$$(P_S)_3=\mp2\zeta\chi A^3\ . \tag{38}$$

Hamano *et al.*[4] have measured pyroelectric charges in the ferroelectric lock-in phase of Rb_2ZnCl_4 and calculated from these data the spontaneous polarization. We have fitted their results by a power law

$$(P_S)_3=M(T'-T)^\beta\ , \tag{39}$$

with $M=0.02\ \mu C/cm^2K$, $T'=222.9$ K, and $\beta=0.47$. These parameters will be used for the interpretation of our nonlinear optical results in the ferroelectric phase.

D. Nonlinear optical effects in the incommensurate phase of Rb_2ZnCl_4

1. *The plane-wave approximation*

In the temperature range where the plane-wave approximation is valid, the local properties of Rb_2ZnCl_4 are sinusoidally modulated. The effective nonlinear coefficient can be written as

$$d_{\rm eff}(x)=D^{(1)}_{\rm eff}(\delta)\cos\left[\frac{2\pi\delta}{3a}x\right]\ , \tag{40}$$

where δ is the temperature-dependent incommensurability parameter and a the length of the paraelectric unit cell in the x direction. From Eq. (40) it follows that the modulation wavelength is

$$\Lambda=3a/\delta\ . \tag{41}$$

A group-theoretical analysis[19] shows that in the incommensurate phase of Rb_2ZnCl_4 the local point-group symmetry should be 1, and hence all the components of the nonlinear optical tensor should be different from zero. However, to date there is no experimental evidence for any rotations of the $ZnCl_4$ tetraeders around the a axis predicted by theory. Therefore, the experimental results indicate that the local symmetry of the incommensurate phase should be better described by the monoclinc point group m. The local nonlinear optical tensor is then, in Voigt notation,

$$\begin{bmatrix} d_{11} & d_{12} & d_{13} & 0 & d_{15} & 0 \\ 0 & 0 & 0 & d_{24} & 0 & d_{26} \\ d_{31} & d_{32} & d_{33} & 0 & d_{35} & 0 \end{bmatrix}\ . \tag{42}$$

With Eq. (40) the nonlinear dielectric polarization can be written as

$$(P_{\rm NL})^{(2\omega)}(x)=\epsilon_0D^{(1)}_{\rm eff}(\delta)\cos\left[\frac{2\pi\delta}{3a}x\right](E^{(\omega)})^2\ . \tag{43}$$

The intensity of the second-harmonic wave in the plane-wave limit is then given by

$$I_{2\omega}=2\left[\frac{\mu_0}{\epsilon_0}\right]^{1/2} I_\omega^2 \frac{D_{\rm eff}^{(1)}(\delta)^2 l^2}{n_\omega^2 n_{2\omega}}\omega^2 \times\frac{1}{4}\left\{j_0^2\left[\left[\Delta k-\frac{2\pi\delta}{3a}\right]\frac{l}{2}\right]+j_0^2\left[\left[\Delta k+\frac{2\pi\delta}{3a}\right]\frac{l}{2}\right] +\cos\left[\frac{2\pi\delta}{3a}l\right] j_0\left[\left[\Delta k-\frac{2\pi\delta}{3a}\right]\frac{l}{2}\right] \times j_0\left[\left[\Delta k+\frac{2\pi\delta}{3a}\right]\frac{l}{2}\right]\right\}, \tag{44}$$

remembering that $j_0(x)=\sin x/x$. It has been shown in Refs. 1 and 20 that for Rb_2ZnCl_4 near T_I,

$$\delta=0.08,\quad a=9.3\ \text{Å}\ .$$

From our work it follows that

$$\Delta k=\pi/l_c=0.2\ \mu\text{m}^{-1}\ .$$

With these data and $\Delta k \ll 2\pi\delta/3a=180\ \mu\text{m}^{-1}$, it is possible to estimate the ratio between the second-harmonic power in the incommensurate and ferroelectric lock-in phases

$$\frac{P_{2\omega}^{\rm inc}}{P_{2\omega}^{C}}=\frac{D_{\rm eff}^{(1)}(\delta)^2}{d_{\rm eff}^2}\left[\frac{\Delta k}{2\pi\delta/3a}\right]^2=1.4\times10^{-6}\frac{D_{\rm eff}^{(1)}(\delta)^2}{d_{\rm eff}^2}\ . \tag{45}$$

As a consequence, we can point out that in the plane-wave limit $P_{2\omega}^{\rm inc}$ is at least 10^6 times smaller than in the ferroelectric phase. It is, furthermore, interesting to note that because of the extremely small modulation period of $P_{2\omega}(y)$ in the incommensurate phase,

$$Y_0=\frac{3a}{\delta\tan\theta}=0.6\ \mu\text{m}\ , \tag{46}$$

the beam-width parameter η, Eq. (17), becomes very large ($\eta>100$ in our experiment), and the second-harmonic power, consequently, independent of the wedge position.

2. *The multisoliton limit and quasi-phase-matching*

In the low-temperature part of the incommensurate phase the plane-wave approximation breaks down and according to Sec. II B 2, the space dependence of the local physical properties of Rb_2ZnCl_4 is no longer sinusoidal but contains higher harmonics. As a consequence, the effective nonlinear optical susceptibility should be expanded in a Fourier series

$$d_{\rm eff}=\sum_{n=1}^{\infty} D_{\rm eff}^{(n)}(\delta)\cos\left[\frac{2\pi\delta}{3a}nx\right]\ . \tag{47}$$

Solving Maxwell's equations with

$$P_{\rm NL}^{(2\omega)}(x)=\epsilon_0\left[\sum_{n=1}^{\infty} D_{\rm eff}^{(n)}(\delta)\cos\left[\frac{2\pi\delta}{3a}nx\right]\right](E^{(\omega)})^2 \tag{48}$$

as the nonlinear source term, we find for the second-harmonic intensity

$$\begin{aligned} I_{2\omega}=2\left[\frac{\mu_0}{\epsilon_0}\right]^{1/2} I_\omega^2\frac{l^2}{n_{2\omega}n_\omega^2}\omega^2\frac{1}{4}\Bigg\{ & D_{\rm eff}^{(1)^2}(\delta)j_0^2\left[\left[\frac{2\pi\delta}{3a}-\Delta k\right]\frac{l}{2}\right]+D_{\rm eff}^{(1)^2}(\delta)j_0^2\left[\left[\frac{2\pi\delta}{3a}+\Delta k\right]\frac{l}{2}\right] \\ & +D_{\rm eff}^{(2)^2}(\delta)j_0^2\left[\left[\frac{4\pi\delta}{3a}-\Delta k\right]\frac{l}{2}\right]+D_{\rm eff}^{(2)^2}(\delta)j_0^2\left[\left[\frac{4\pi\delta}{3a}+\Delta k\right]\frac{l}{2}\right] \\ & +2D_{\rm eff}^{(1)}(\delta)\cos\left[\frac{2\pi\delta}{3a}l\right]j_0\left[\left[\frac{2\pi\delta}{3a}-\Delta k\right]\frac{l}{2}\right]j_0\left[\left[\frac{2\pi\delta}{3a}+\Delta k\right]\frac{l}{2}\right] \\ & +2D_{\rm eff}^{(2)}(\delta)\cos\left[\frac{4\pi\delta}{3a}l\right]j_0\left[\left[\frac{4\pi\delta}{3a}-\Delta k\right]\frac{l}{2}\right]j_0\left[\left[\frac{4\pi\delta}{3a}+\Delta k\right]\frac{l}{2}\right] \\ & +2D_{\rm eff}^{(1)}(\delta)D_{\rm eff}^{(2)}(\delta)\cos\left[\frac{3\pi\delta}{3a}l\right]j_0\left[\left[\frac{2\pi\delta}{3a}+\Delta k\right]\frac{l}{2}\right]j_0\left[\left[\frac{4\pi\delta}{3a}-\Delta k\right]\frac{l}{2}\right] \\ & +2D_{\rm eff}^{(1)}(\delta)D_{\rm eff}^{(2)}(\delta)\cos\left[\frac{3\pi\delta}{3a}l\right]j_0\left[\left[\frac{2\pi\delta}{3a}-\Delta k\right]\frac{l}{2}\right]j_0\left[\left[\frac{4\pi\delta}{3a}+\Delta k\right]\frac{l}{2}\right]+\cdots\Bigg\}, \end{aligned} \tag{49}$$

remembering that $j_0(x)=\sin x/x$. Approaching T_C, the incommensurability parameter δ rapidly decreases[1] and, according to Eq. (41), the wavelength of the incommensurate modulation increases. Therefore, we would like to estimate whether this increased period could lead to quasi-phase-matching of the fundamental and second-harmonic waves. Quasi-phase-matching would considerably increase the conversion efficiency. In fact, as can be seen from Fig. 2, when the phase synchronism conditions

$$\Delta k=\pm m\frac{2\pi\delta}{3a},\quad m=1,2,3,\ldots \tag{50}$$

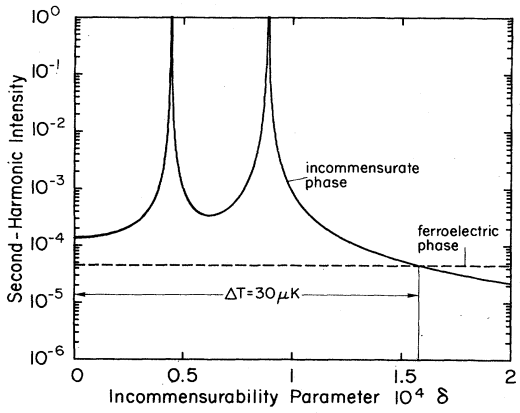

FIG. 2. Second-harmonic intensity as a function of the incommensurability parameter δ. The envelope of the second-harmonic intensity function calculated from Eq. (49), shown as a solid line, is compared to the second-harmonic intensity in the ferroelectric phase at $T=190$ K. The two peaks occur for $\Delta k = m(2\pi\delta/3a)$ with $m=1$ and $m=2$, respectively. The temperature range where the second-harmonic intensity would be larger than in the ferroelectric phase due to quasi-phase-matching is $\Delta T=30\,\mu$K.

are fulfilled, the generated second-harmonic intensity has sharp maxima. Using Eq. (50) we find for $m=1$ with $\Delta k=0.2\,\mu\text{m}^{-1}$,

$$\delta=0.9\times10^{-4}\ .$$

The task of determining the temperature, where phase matching might first occur (i.e., where $\delta=0.9\times10^{-4}$), can be solved by relating $\delta(T)$ to the temperature dependence of the soliton density n_s defined by Kind in Ref. 21 as the ratio between the soliton width b and the intersoliton distance x_0,

$$n_s=b/x_0\ . \tag{51}$$

In fact, as $x_0=\Lambda/6$ (see Fig. 1), where $\Lambda=3a/\delta$ is the modulation wavelength of the incommensurate structure, one obtains

$$n_s(T)=\frac{2b(T)\delta(T)}{a(T)}\ . \tag{52}$$

Assuming that the soliton width and lattice constant a are temperature independent, we have in a first approximation

$$n_s(T)=\frac{2n_s(T_I)}{\delta(T_I)}\delta(T)\ . \tag{53}$$

With the experimental soliton density data given by Blinc *et al.* in Ref. 22 the temperature T_{PM} where phase matching might first occur is

$$T_{\text{PM}}=T_C+0.01\text{ mK}\ . \tag{54}$$

The temperature stability required for phase matching can easily be calculated from the condition

$$\Delta\delta\lesssim 3a/l=10^{-6} \tag{55}$$

with $a=9.3$ Å and $l=3$ mm.

Using relation (53) we get

$$|\Delta T_{\text{PM}}|\leq 0.1\,\mu\text{K}\ . \tag{56}$$

We have furthermore calculated that the temperature range, where the second-harmonic intensity in the incommensurate phase becomes larger than the second-harmonic intensity in the ferroelectric phase because of the quasi-phase-matching effect, is confined to an interval of 30 μK (see Fig. 2). From these estimations it is clear that quasi-phase-matching cannot be observed experimentally. Finally we want to point out that all previous calculations assume plane electromagnetic waves. In the incommensurate phase, however, the refractive indices as well as the electromagnetic wave amplitudes are modulated with a wavelength corresponding to the superstructure of the material. This leads to a number of new optical effects which are characteristic of the incommensurate structure and which were predicted theoretically by Golovko and Levanyuk.[23] Nevertheless, their estimation of the second-harmonic intensity in the incommensurate phase agrees with the result of our calculations based on our measurement of the coherence length in the ferroelectric phase (see Sec. IV B).

E. Structural changes in the incommensurate phase of Rb_2ZnCl_4 due to defect-induced pinning of solitons

In the foregoing, all calculations were based on the assumption that the crystal is free of defects. In real samples of Rb_2ZnCl_4, however, defects interact with the phase solitons and lead to a unipolar domain structure as was pointed out by Arutyunyan *et al.*[12] Symmetry in each domain can be described by the point group $mm2$ of the ferroelectric lock-in phase. Because of the repulsive interaction of phase solitons, the pinning effect appears only in the low-temperature part of the incommensurate phase where the intersoliton distance x_0 increases considerably. For instance, electro-optic measurements[11] have shown that the soliton lattice becomes "soft" at approximately T_C+16 K. Furthermore the unipolarity of the domain structure is well documented by the measurement of a pyroelectric charge in the incommensurate phase near T_C.[4] As a consequence, all the harmonics allowed by the symmetry of the polar lock-in phase can also occur in the incommensurate phase below T_C+16 K.

F. Nonlinear optical effect in the ferroelectric lock-in phase

In the ferroelectric lock-in phase the point-group symmetry is $mm2$ and the nonlinear optical tensor is given by

$$\begin{bmatrix} 0 & 0 & 0 & 0 & d_{15} & 0 \\ 0 & 0 & 0 & d_{24} & 0 & 0 \\ d_{31} & d_{32} & d_{33} & 0 & 0 & 0 \end{bmatrix}. \tag{57}$$

The second-harmonic generation in the ferroelectric phase of Rb_2ZnCl_4 is basically a third-order nonlinear optical effect biased by the spontaneous polarization $(P_S)_3$. In the paraelectric phase of Rb_2ZnCl_4 the lowest-order nonlinear optical effects are described by the fourth-rank tensor

components d_{ijkl} [see Eq. (5)]. The nonlinear polarization responsible for third-harmonic generation is given by

$$(P_{\mathrm{NL}})_i^{(3\omega)}=\epsilon_0 d_{ijkl}^{(-3\omega;\omega,\omega,\omega)}E_j^{(\omega)}E_k^{(\omega)}E_l^{(\omega)} \tag{58}$$

and, according to Eq. (6),

$$E_i^{(3\omega)}=\frac{1}{\epsilon_0}\delta_{ijkl}^{(-3\omega;\omega,\omega,\omega)}P_j^{(\omega)}P_k^{(\omega)}P_l^{(\omega)}\ , \tag{59}$$

where $\delta_{ijkl}^{(-3\omega;\omega,\omega,\omega)}$ is given by relation (7).

In the polar ferroelectric phase the nonlinear optical effects can be described by the same relation (59) biased by the dc polarization $(P_S)_3$, giving a relation for the second-order nonlinearity,

$$E_i^{(2\omega)}=\frac{1}{\epsilon_0}\delta_{ijk3}^{(-2\omega;\omega,\omega,0)}P_j^{(\omega)}P_k^{(\omega)}(P_S)_3\ . \tag{60}$$

This has to be compared with the usual second-order nonlinear equation (9), where we set $\omega=\omega_0=\omega_p$. Therefore,

$$\delta_{ijk}^{(-2\omega;\omega,\omega)}=\delta_{ijk3}^{(-2\omega;\omega,\omega,0)}(P_S)_3\ . \tag{61}$$

Assuming $\delta_{ijk3}^{(-2\omega;\omega,\omega,0)}$ as temperature independent, one can conclude that the temperature dependence of $\delta_{ijk}^{(2\omega)}$ is determined by the temperature dependence of the spontaneous polarization.

III. EXPERIMENTAL

The experimental setup is schematically shown in Fig. 3. The light source at the fundamental wavelength ($\lambda_0=1064$ nm) was a Q-switched Nd:YAG laser (YAG denotes yttrium-aluminum-garnet) (Spectra-Physics model 3000). The sample was mounted in an optical clipping cryostat. The lens L_1 focused the laser beam into the nonlinear crystal and L_2 collimated the generated second harmonic ($\lambda_0=532$ nm), which was detected by a photomultiplier (RCA 1 P28). A dichroic beam splitter and an infrared-absorption filter (BG 18) placed in front of the detector blocked the fundamental wave. The light polarization directions were adapted to the geometry of the nonlinear interaction by means of a polarization rotator and a Glan prism. The optical cryostat was mounted onto a translation stage which could be translated perpendicularly to the beam direction by a computer-controlled stepper motor. The crystal position y was measured with a high-resolution 1-μm-length measuring system (Heidenhain model LS 903). The second-harmonic signal was exponentially averaged in a gated integrator (EG&G PAR model 165), whose output was subsequently stored by a

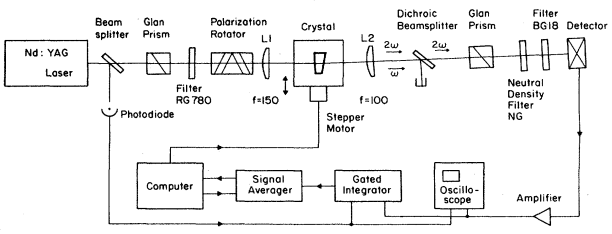

FIG. 3. Experimental setup for measuring nonlinear optical coefficients using the wedge technique.

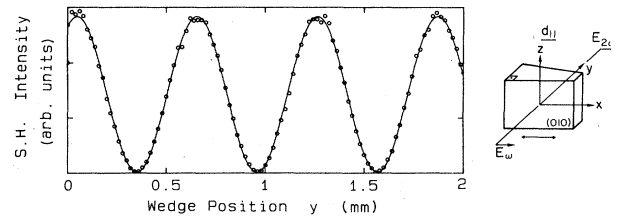

FIG. 4. Typical second-harmonic fringes obtained for α-quartz with the corresponding sample orientation. Open circles are experimental values, solid line is theoretical curve calculated from Eq. (15).

1024-channel signal averager (EG&G, PAR model 4202). Each one of the 1024 channels could be identified with a corresponding translation-stage position y.

As the standard reference material, we used an α-quartz crystal. For determining the temperature dependence of the nonlinear optical coefficients of Rb_2ZnCl_4 we measured the ratio

$$\frac{d_{\mathrm{eff}}}{d_{11}^{Q}}=\frac{d_{\mathrm{eff}}(Rb_2ZnCl_4)}{d_{11}(\mathrm{quartz})}$$

at each temperature. Figure 4 gives an example of the precision of the nonlinear optical measurement. We plot the second-harmonic power as a function of the wedge displacement for the reference material α-SiO_2. The crystal orientation is also shown. Experimental points are compared with the theoretical expression [Eq. (15)] shown as a solid line. The coherence length l_c calculated from the period of $P_{2\omega}(y)$,

$$l_c=\frac{\pi c}{2\,|\,n_{2\omega}-n_{\omega}\,|\,\omega}=(21.0\pm0.2)\ \mu\mathrm{m}\ ,$$

compares well with the value $l_c=20.64$ μm given by Jerphagnon and Kurtz.[24]

The sensitivity of our experimental setup was high enough to measure second-harmonic signals 10^6 times lower than the one generated in the α-quartz crystal. For the temperature-dependence measurements we could control the temperature with an accuracy of better than ±0.25 K. The Rb_2ZnCl_4 wedge was a melt-grown sample prepared in our laboratory.[9] The dimensions of the crystal wedge [wedge angle $\theta=(3.66\pm0.02)°$] are $A\times B\times C=3\times10\times5.9$ mm^3. The crystal orientation is shown in Fig. 5.

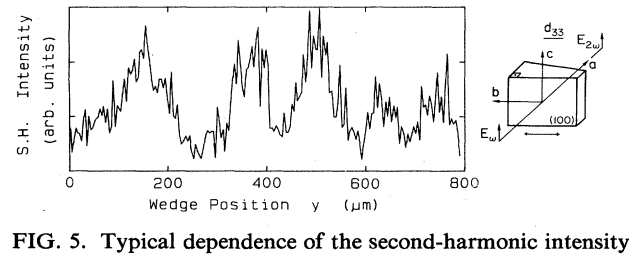

FIG. 5. Typical dependence of the second-harmonic intensity on the wedge position in the incommensurate phase of Rb_2ZnCl_4.

IV. RESULTS

A. Nonlinear optical properties in the incommensurate phase of Rb_2ZnCl_4

In the incommensurate phase of Rb_2ZnCl_4, with no polarizing dc electric field applied, second-harmonic signals corresponding to the geometries d_{24}, d_{32}, and d_{33} could be measured below $T_C + 4$ K. Figure 5 shows a typical position dependence of the second-harmonic power in the incommensurate phase of the crystal. As it is impossible to fit Eq. (15) to the experimental data, we have averaged the second-harmonic power

$$M = \frac{1}{L}\int_0^L P_{2\omega}(y)dy \tag{62}$$

to get a measure for the optical nonlinearity of the sample. L is the total crystal translation along the y direction (typically $L = 1$ mm in our experiments).

In Fig. 6 we have plotted the temperature dependence of $\log_{10}(M/M_Q)$ for geometries using the nonlinear coefficients d_{24}, d_{32}, and d_{33}. According to (62), M_Q designates the spatial average of the second-harmonic power for the standard quartz crystal. It is clear from Fig. 6 that second-harmonic generation is not only observed in the ferroelectric phase below $T_C = 187$ K but also in the incommensurate phase. A pronounced thermal hysteresis of approximately 4 K is observed by measuring M/M_Q on cooling and heating cycles. Finally, it should be pointed out that in the ferroelectric phase, without any polarizing electric dc field applied, M/M_Q is about 4 orders of magnitude larger than in the incommensurate phase. An electric polarizing field has no influence on the space dependence of the second-harmonic power observed in the incommensurate phase. It is worthwhile to note that in a logarithmic scale, our measured M/M_Q points lie on the same curve for all three geometries in which the nonlinear susceptibilities d_{33}, d_{32}, and d_{24} were involved.

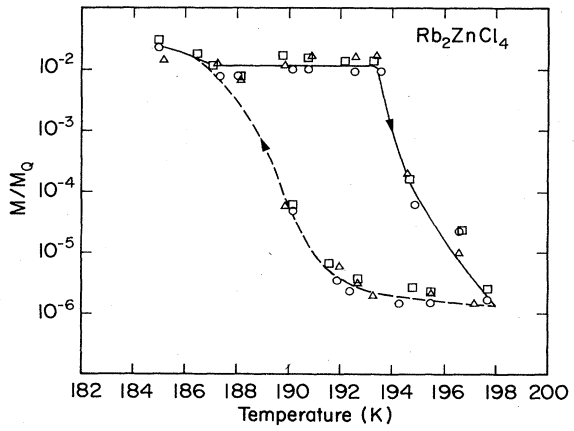

FIG. 6. Temperature hysteresis of M/M_Q around T_c in Rb_2ZnCl_4. M designates the spatial average of the second-harmonic intensity for Rb_2ZnCl_4 crystal and M_Q the corresponding average for the standard quartz crystal. Open squares are M/M_Q data using the geometry for d_{33}, open circles are M/M_Q data using the geometry for d_{32}, and open triangles are M/M_Q data using the geometry for d_{24}.

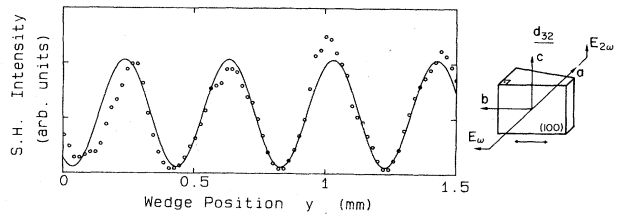

FIG. 7. Typical second-harmonic fringes obtained for Rb_2ZnCl_4 in the ferroelectric lock-in phase at $T = 179$ K. Open circles are experimental values, solid line is theoretical curve calculated from Eq. (15).

B. Nonlinear optical properties in the ferroelectric lock-in phase of Rb_2ZnCl_4

The nonlinear optical coefficients d_{32}, d_{33}, and d_{24} were measured in the temperature range from 95 to 200 K upon heating. To remove the domain structure a dc electric field on the order of 3.5 kV/cm was applied along the polar c axis. Figure 7 shows the space dependence of the second-harmonic power in the ferroelectric phase at 179 K. $P_{2\omega}(y)$ is periodic and can be fitted according to Eq. (15). In Figs. 8 and 9 we have plotted the temperature

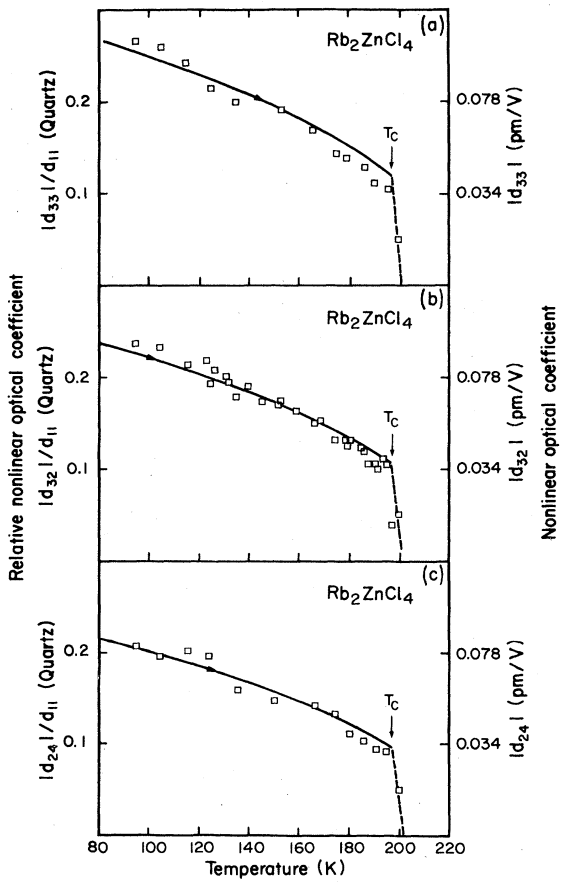

FIG. 8. Temperature dependence of the nonlinear optical coefficients (a) $|d_{33}|$, (b) $|d_{32}|$, and (c) $|d_{24}|$ for Rb_2ZnCl_4 at $\lambda_0 = 1064$ nm. Open squares are experimental values, solid line is numerical fit using the spontaneous polarization data.

TABLE I. Nonlinear optic coefficients, coherence lengths, and refractive-index dispersion of Rb_2ZnCl_4 at $T=100$ and 190 K.

Temperature (K)	Nonlinear optical coefficients d_{33} (pm/V)	d_{32} (pm/V)	d_{24} (pm/V)	Coherence lengths l_{c33} (μm)	l_{c32} (μm)	l_{c24} (μm)	Refractive index dispersion $n_3(2\omega)-n_3(\omega)$ $=\lambda_0/(4\times l_{c33})$	$n_3(2\omega)-n_2(\omega)$ $=\lambda_0/(4\times l_{c32})$	$n_2(2\omega)-\frac{n_3+n_2}{2}(\omega)$ $=\lambda_0/(4\times l_{c24})$
100	0.085 ±0.015	0.075 ±0.015	0.069 ±0.015	14.5 ±0.2	13.5 ±0.2	15.5 ±0.2	0.0183 ±0.0003	0.0197 ±0.0003	0.0172 ±0.0003
190	0.045 ±0.010	0.041 ±0.010	0.037 ±0.010	14.5 ±0.2	12.5 ±0.2	15.5 ±0.2	0.0183 ±0.0003	0.0213 ±0.0003	0.0172 ±0.0003

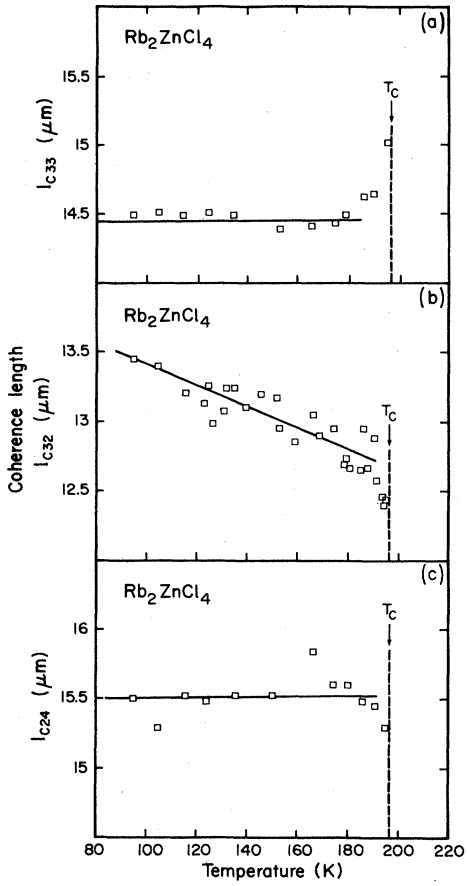

FIG. 9. Temperature dependence of the coherence lengths (a) $l_{c33}=\lambda_0/4\,|\,n_3(2\omega)-n_3(\omega)\,|$, (b) $l_{c32}=\lambda_0/4\,|\,n_3(2\omega)-n_2(\omega)\,|$, and (c) $l_{c24}=\lambda_0/4\,|\,n_2(2\omega)-[(n_2+n_3)/2](\omega)\,|$.

dependence of the nonlinear optic coefficients $|d_{33}|/d_{11}^{Q}$, $|d_{32}|/d_{11}^{Q}$, and $|d_{24}|/d_{11}^{Q}$ and the coherence lengths l_{c32}, l_{c33}, and l_{c24}, respectively. Table I resumes the nonlinear optic coefficients, coherence lengths, and refractive-index dispersion at 100 and 190 K. In the whole temperature range $100 < T < 190$ K we find

$$|d_{33}| > |d_{32}| > |d_{24}| \ .$$

All three nonlinear optical coefficients d_{33}, d_{32}, and d_{24} increase in the ferroelectric phase with decreasing temperature. From Fig. 8 it follows that $d_{32}(T)$, $d_{33}(T)$, and $d_{24}(T)$ can be compared well with the temperature dependence of the spontaneous polarization $(P_S)_3$. While the coherence lengths l_{c33} and L_{c24} remain nearly constant in the ferroelectric phase, l_{c32} continuously decreases from 13.5 μm at 100 K to approximately 12.5 μm at 190 K. The ferroelectric-incommensurate phase-transition temperature has been measured to be at $T_C(E)=(196.5\pm0.5)$ K (see Sec. IV A). The electric-field-induced shift of the phase-transition temperature for $E=3.5$ kV/cm is $\Delta T_C=(3\pm1)$ K and thus $dT_C/dE=(0.9\pm0.4)$ K cm/kV. This value is larger than $dT_C/dE=0.35$ K cm/kV calculated by Hamano *et al.* from pyroelectric measurements[4] and $dT_C/dE=0.67$ K cm/kV obtained in electro-optic experiments.[11]

V. DISCUSSION

A. Interpretation of the experimental results in the incommensurate phase of Rb_2ZnCl_4

The random space distribution of the second-harmonic power (Fig. 5) in the incommensurate phase below 200 K, the broad temperature hysteresis around T_C, and the fact that we could only measure second-harmonic signals corresponding to tensor components allowed by the symmetry of the polar lock-in phase, leads us to the conclusion that the measured nonlinear optical effects in the incommensurate phase of Rb_2ZnCl_4 are due to the defect-induced pinning of solitons. Furthermore, as in the ferroelectric phase $P_{2\omega}^{C}=10^{-2}P_{2\omega}(\text{quartz})$ (see Fig. 8) the second-harmonic power caused by a perfect incommensurate structure is, according to Eq. (45),

$$P_{2\omega}^{\text{inc}}<10^{-7}P_{2\omega}(\text{quartz}) .$$

Such intensities could not be resolved with our experimental setup. The results agree with the nonlinear optical experiments on K_2SeO_4 carried out by Arutyunyan *et al.*[12] They measured in the incommensurate phase of K_2SeO_4 only second-harmonic signals corresponding to nonlinear optical coefficients allowed by the symmetry of the ferroelectric lock-in phase and observed the same broad temperature hysteresis around T_C as we did in Rb_2ZnCl_4. Finally we must point out that our results disagree with those given by Vtyurin *et al.* in $(NH_4)_2BeF_4$.[13] These authors could resolve in the incommensurate phase of $(NH_4)_2BeF_4$ second-harmonic signals corresponding to the nonlinear optical coefficients d_{22}, d_{23}, and d_{33}, where d_{22} and d_{23} are only allowed by the symmetry of the point group 1, which the authors attributed to the structure of the incommensurate phase. The most striking fact in their measurements was that the magnitude of the second-harmonic signals they observed in the incommensurate phase was comparable to the second-harmonic intensity in the ferroelectric lock-in phase. They interpreted the high second-harmonic intensities by quasi-phase-matching smeared out over the whole incommensurate temperature range. We have however seen in Sec. II D 2 that, in Rb_2ZnCl_4, quasi-phase-matching would enhance the second-harmonic intensity only in a temperature range of 30 μK.

B. Interpretation of the nonlinear optical properties of Rb_2ZnCl_4 in the ferroelectric lock-in phase

Figure 10 shows the temperature dependences of the Miller coefficients δ_{33}, δ_{32}, and δ_{24}, which were calculated from our measured nonlinear optical coefficients d_{33}, d_{32}, and d_{24} by using the refractive-index data reported in Ref. 10. The experimental result agrees very well with Eq. (61) for all three Miller δ coefficients δ_{33}, δ_{32}, and δ_{24}. This allows the determination of the fourth-rank Miller δ coefficients [with the data for $(P_S)_3(T)$ from Ref. 4]

$$\delta_{3333}=(1.7\pm0.1)\frac{m^4}{C^2} ,$$

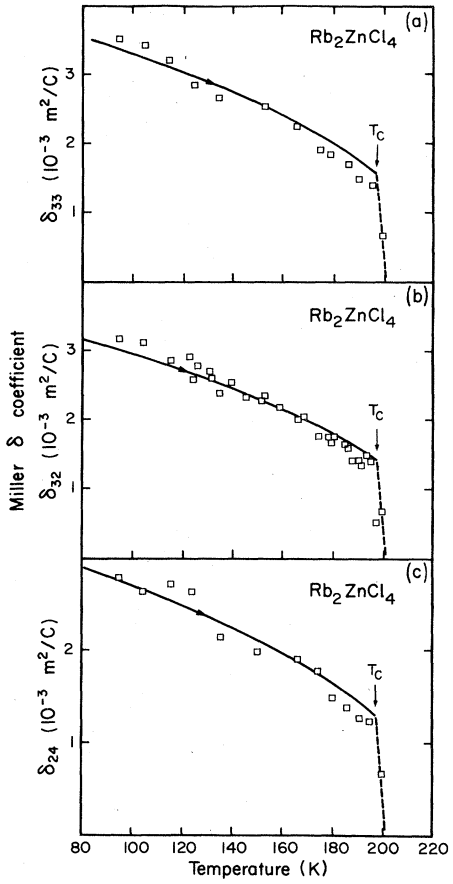

FIG. 10. Temperature dependence of the Miller δ coefficients (a) $|\delta_{33}|$, (b) $|\delta_{32}|$, and (c) $|\delta_{24}|$ for Rb_2ZnCl_4 at $\lambda_0=1064$ nm. Open squares are calculated from nonlinear optical coefficients using Eq. (10), solid line is theoretical curve (proportional to the spontaneous polarization).

$$\delta_{3223}=(1.5\pm0.1)\frac{m^4}{C^2} ,$$

$$\delta_{3233}=(0.7\pm0.1)\frac{m^4}{C^2} .$$

Table II compares the nonlinear d and δ coefficients as well as the spontaneous polarization of Rb_2ZnCl_4 to the equivalent quantities of some other materials.

The stress-free linear electro-optic coefficient consists of three contributions,

$$r=r_a+r_o+r_e . \tag{63}$$

The above-mentioned terms are due to field-induced electronic (r_e) and lattice polarizations, where the latter consist of acoustic- (r_a) and optic- (r_o) phonon-mode contributions, respectively. In the principal-axis system, the optical $d_{ijk}^{(-\omega;\omega,0)}$ coefficients describing electric-field-induced changes of the Fresnel ellipsoid are related to the free electro-optic coefficients r_{ijk} by[15]

$$d_{ijk}^{(-\omega;\omega,0)}=-n_i^2 r_{ijk} n_j^2 , \tag{64}$$

where n_i and n_j are refractive indices. The corresponding Miller δ coefficients are

TABLE II. Nonlinear optical coefficients, Miller δ, coefficients and spontaneous polarization of some ferroelectric materials at room temperature (Ref. 25) and of Rb_2ZnCl_4 at 190 K.

Material	Nonlinear optical coefficient (10^{-12} m/V)	Miller δ coefficient (10^{-2} m^2/C)	Spontaneous polarization (10^{-2} C/m^2)
$BaMgF_4$	$d_{32}=$ 0.065	$\delta_{32}=$ 0.56	7.7
Rb_2ZnCl_4	$d_{33}=$ 0.045 $d_{32}=$ 0.041 $d_{24}=$ 0.037	$\delta_{33}=$ 0.18 $\delta_{32}=$ 0.16 $\delta_{24}=$ 0.14	0.1
KDP	$d_{36}=$ 0.63	$\delta_{36}=$ 4.0	7.3
$NaNO_2$	$d_{32}=$ 2.9	$\delta_{32}=$11.5	8.6
$KNbO_3$	$d_{33}=$27	$\delta_{33}=$ 6.3	41

$$\delta_{ijk}^{(-\omega;\omega,0)}=-r_{ijk}\frac{n_i^2 n_j^2}{\epsilon_0(n_i^2-1)(n_j^2-1)(\epsilon_k^{(\omega=0)}-1)} . \quad (65)$$

$\epsilon_k^{(\omega=0)}$ is the static dielectric constant along the k direction in the principal-axis system. In Table III the nonlinear optical Miller $\delta^{(-2\omega,\omega,\omega)}$ are compared to $\delta^{(-\omega,\omega,0)}$ where the static dielectric constant data are taken from Ref. 10.

The contribution of the optic-phonon modes to the nonlinear optical $d_{ijk}^{(-\omega,\omega,0)}$ coefficients is given by

$$d_{ijk}^0=\sum_n \rho_{ij}^n \frac{dQ^n}{dE_k} , \quad (66)$$

where Q^n is the atomic displacement induced by the optic-phonon mode n and ρ_{ij}^n the Raman tensor element corresponding to the nth mode. Only those phonon modes which are Raman ($\rho_{ij}^n\neq 0$) and infrared ($dQ^n/dE_k\neq 0$) active can contribute to the electro-optic effect. Neglecting the internal-vibrational degrees of freedom in the $ZnCl_4$ groups, 48 phonon modes exist in Rb_2ZnCl_4, which transform according to[19]

$$14\Sigma_1+10\Sigma_2+10\Sigma_3+14\Sigma_4 .$$

Σ_1, Σ_2, Σ_3, and Σ_4 are irreducible representations of the space group $Pna2_1$ on the Σ line. It can be shown[26] that the optic-phonon modes which transform according to Σ_3 and Σ_4 are both Raman and infrared active. The corresponding Raman tensors are

$$\Sigma_3:\begin{bmatrix}0&0&\rho_{13}\\0&0&0\\\rho_{31}&0&0\end{bmatrix},\quad \Sigma_4:\begin{bmatrix}0&0&0\\0&0&\rho_{23}\\0&\rho_{32}&0\end{bmatrix} .$$

From the foregoing one can conclude that only the electro-optic coefficients d_{42} and d_{51} contain optic-phonon contributions. For d_{13}, d_{23}, and d_{33} only acoustic phonons and electronic excitations contribute to the nonlinear polarizability. With the results resumed in Table III it is clear that acoustic-phonon contributions are small in the case of $\delta_{333}^{(-\omega,\omega,0)}$ and large in the case of $\delta_{223}^{(-\omega,\omega,0)}$. The contribution of optic- and acoustic-phonon modes to $\delta_{322}^{(-\omega,\omega,0)}$ is large compared to the electronic contribution.

VI. CONCLUSION

We have measured the nonlinear optical properties of Rb_2ZnCl_4 in the incommensurate and ferroelectric lock-in phases of Rb_2ZnCl_4 by using the wedge technique. In the incommensurate phase we could only resolve second-harmonic signals due to nonlinear optical coefficients allowed by the symmetry of the ferroelectric phase. We conclude that the observed effect is due to the presence of a unipolar defect-induced domain structure with the point-group symmetry $mm2$ of the ferroelectric phase. We were able to show that the second-harmonic intensity generated in a defect-free incommensurate structure is 10^7 times smaller than the second-harmonic intensity generat-

TABLE III. δ and d coefficients of Rb_2ZnCl_4 at $T=186$ K. The low-frequency electro-optic coefficients are compared to the nonlinear coefficients at optical frequencies.

Electro-optic effect		Nonlinear optical contribution	
$\delta_{ijk}^{(-\omega;\omega,0)}$ ($m^2/C\times 10^{-3}$)	$d_{ijk}^{(-\omega;\omega,0)}$ (pm/V)	$\delta_{ijk}^{(-2\omega;\omega,\omega)}$ ($m^2/C\times 10^{-3}$)	$d_{ijk}^{(-2\omega;\omega,\omega)}$ (pm/V)
$\lvert\delta_{333}\rvert=1.6$	$\lvert d_{333}\rvert=0.63$	$\lvert\delta_{333}\rvert=2$	$\lvert d_{333}\rvert=0.044$
$\lvert\delta_{322}\rvert=9$	$\lvert d_{322}\rvert=0.48$	$\lvert\delta_{322}\rvert=1.6$	$\lvert d_{322}\rvert=0.039$
$\lvert\delta_{232}\rvert=9$	$\lvert d_{232}\rvert=0.48$	$\lvert\delta_{232}\rvert=1.5$	$\lvert d_{232}\rvert=0.036$
$\lvert\delta_{223}\rvert=8$	$\lvert d_{223}\rvert=3.07$	$\lvert\delta_{223}\rvert=1.5$	$\lvert d_{223}\rvert=0.036$

ed in the reference quartz crystal and therefore too small for detection with our experimental setup. Furthermore, we estimated that quasi-phase-matching of the second-harmonic and fundamental waves in the incommensurate phase of Rb_2ZnCl_4 can occur within a temperature range of only $T_C < T_{PM} < T_C + 0.01$ mK. Moreover, the temperature range, where the second-harmonic intensity in the incommensurate phase becomes larger than the second-harmonic intensity in the ferroelectric phase because of the quasi-phase-matching effect is confined to an interval of 0.03 mK.

In the ferroelectric lock-in phase our measured nonlinear optical coefficients are proportional to the spontaneous polarization or proportional to A^3 where A is the amplitude of the order parameter. Thus, the Miller δ coefficients δ_{33}, δ_{32}, and δ_{24} could be related to the fourth-rank Miller δ coefficients δ_{3333}, δ_{3233}, and δ_{3223} by using previously measured data for the spontaneous polarization $(P_S)_3$.

ACKNOWLEDGMENTS

The authors would like to thank H. Arend and H. Wuest for growing the crystal and J. Hajfler for polishing the sample. This work was supported in part by the Swiss National Science Foundation.

[1]H. Mashiyama, S. Tanisaki, and K. Hamano, J. Phys. Soc. Jpn. **51**, 2538 (1982).
[2]M. Wada, A. Sawada, and Y. Ishibashi, J. Phys. Soc. Jpn. **47**, 1185 (1979).
[3]R. Blinc, P. Prelovsek, and R. Kind, Phys. Rev. B **27**, 5404 (1983).
[4]K. Hamano, Y. Ikeda, T. Fujimoto, K. Ema, and S. Hirotsu, J. Phys. Soc. Jpn. **49**, 2278 (1980).
[5]H.-G. Unruh, J. Phys. C **16**, 3245 (1983).
[6]A. Levstik, P. Prelovsek, C. Filipic, and B. Zeks, Phys. Rev. B **25**, 3416 (1982).
[7]H. Mashiyama and H.-G. Unruh, J. Phys. C **16**, 5009 (1983).
[8]S. Sawada, Y. Shiroishi, A. Yamamoto, M. Takashige, and M. Matsuo, J. Phys. Soc. Jpn. **43**, 2099 (1977).
[9]P. Günter, R. Sanctuary, F. Rohner, H. Arend, and W. Seidenbusch, Solid State Commun. **37**, 883 (1981).
[10]P. Günter, R. Sanctuary, and F. Rohner, Phys. Status Solidi A **70**, 583 (1982).
[11]R. Sanctuary and P. Günter, Phys. Status Solidi A **84**, 103 (1984).
[12]A. M. Arutyunyan, B. Brezina, S. Kh. Esayan, and V. V. Lemanov, Fiz. Tverd. Tela (Leningrad) **24**, 1434 (1982) [Sov. Phys.—Solid State **24**, 814 (1982)].
[13]A. I. Vtyurin, V. F. Shabanov, and K. S. Alexandrov, Zh. Eksp. Teor. Fiz. **77**, 2358 (1979) [Sov. Phys.—JETP **50**, 1137 (1979)].
[14]R. C. Miller, Appl. Phys. Lett. **5**, 17 (1964).
[15]M. DiDomenico and S. H. Wemple, J. Appl. Phys. **40**, 720 (1969); **40**, 735 (1969).
[16]G. D. Boyd, H. Kasper, and J. H. McFee, IEEE J. Quantum Electron. **QE-7**, 563 (1971).
[17]D. G. Sannikov and A. P. Levanyuk, Fiz. Tverd. Tela (Leningrad) **20**, 1005 (1978) [Sov. Phys.—Solid State **20**, 580 (1978)].
[18]W. L. McMillan, Phys. Rev. B **14**, 1496 (1976).
[19]M. Iizumi, J. D. Axe, G. Shirane, and K. Shimaoka, Phys. Rev. B **15**, 4392 (1977).
[20]*Landolt-Börnstein, New Series,* edited by K.-H. Hellwege and A. M. Hellwege (Springer-Verlag, Berlin, 1982), Vol. III/16b, p. 123.
[21]R. Blinc, V. Rutar, B. Topic, F. Milia, I. P. Alexandrova, A. S. Chaves, and R. Gazzinelli, Phys. Rev. Lett. **46**, 1406 (1981).
[23]V. A. Golovko and A. P. Levanyuk, Zh. Eksp. Teor. Fiz. **77**, 1556 (1979) [Sov. Phys.—JETP **50**, 780 (1979)].
[24]J. Jerphagnon and S. K. Kurtz, J. Appl. Phys. **41**, 1667 (1970).
[25]*Landolt-Börnstein, New Series,* Ref. 20, Vols. III/3 and III/11.
[26]W. G. Fateley, F. R. Dollish, N. T. McDevitt, and F. F. Bentley, *Infrared and Raman Selection Rules for Molecular and Lattice Vibrations* (Wiley-Interscience, New York, 1972).